

# Thyroid Cancer Dosimetry Using Clearance Fitting

Eli E. Furhang, Steven M. Larson, Puangrat Buranapong and John L. Humm

Departments of Medical Physics and Nuclear Medicine, Memorial Sloan Kettering Cancer Center, New York, New York; and Division of Nuclear Medicine, Department of Radiology, Siriraj Hospital, Mahidol University, Bangkok, Thailand

Since 1962, Memorial Sloan Kettering Cancer Center has used an individually optimized dosimetry method for patients with thyroid carcinoma undergoing radioiodine therapy. This traditional dosimetry method involves a determination of the maximum tolerated activity or the activity that will deliver 2 Gy to the blood ( $A_{\max}$ ), and the corresponding ablative lesion dose ( $D_{\text{lesion}}$ ). However, the traditional calculations of  $A_{\max}$  and  $D_{\text{lesion}}$  were based on empirical assumptions. The objective of this work was to develop a dosimetry method that eliminates these assumptions by incorporating patient kinetics and that is not restricted to  $^{131}\text{I}$  as a tracer and therapeutic agent. **Methods:** Patient kinetics were incorporated into the dosimetry algorithm by fitting parameters to patient clearance measurements. The radioiodines  $^{123}\text{I}$ ,  $^{124}\text{I}$ ,  $^{125}\text{I}$  and  $^{131}\text{I}$  were accommodated as tracers and therapeutic agents by incorporating their physical half lives and by precalculating photon-absorbed fractions for these radionuclides for several thousand patient geometries using Monte Carlo simulations. **Results:**  $A_{\max}$  and  $D_{\text{lesion}}$  have been calculated using the traditional and new method for a group of patients, and errors associated with each of the above assumptions were examined. Assuming that the initial blood activity is distributed instantaneously in 5 L was found to introduce an error in  $A_{\max}$  of up to 30%, whereas assuming physical decay beyond the last data point introduced an error of up to 50%. **Conclusion:** Individualized fitting of clearance data is a practical method to accurately account for inter-patient kinetics variations. The substitution of standard kinetics beyond measured data might lead to substantial errors in estimating  $A_{\max}$  and  $D_{\text{lesion}}$ . In addition, gamma camera images, rather than neck probe readings, should be used to determine lesion uptakes for thyroid cancer patients.

**Key Words:** radioiodine; thyroid cancer; dosimetry; lesion uptake

**J Nucl Med 1999; 40:131-136**

There are numerous articles that summarize the philosophy of radioiodine dosimetry procedures in the treatment of thyroid cancer (1-6). Two general approaches appear to be in common practice. The first involves administration of a therapeutic amount of  $^{131}\text{I}$ , regardless of the individual patient blood pharmacokinetics or lesion uptake. The second approach involves administration of a tracer amount of  $^{131}\text{I}$

to determine the individual patient radioiodine pharmacokinetics and lesion uptake. The data are then used to calculate the maximum tolerated dose to blood and the dose per unit administered activity to the lesion. The approach developed in this report is most similar to the second approach, as developed by Benua et al. (1).

The maximum activity that can be administered to a patient,  $A_{\max}$ , is defined as the administered activity that will result in an absorbed dose of 2 Gy to blood, corresponding to the onset of leukopenia and thrombocytopenia (1).  $A_{\max}$  is obtained using a thyroid dosimetry study, which consists of administering a tracer activity ( $A_{\text{tracer}}$ ) and then monitoring the radioiodine kinetics in blood and whole body. The blood dose consists of two components: the  $\beta$  dose, estimated from the kinetics of the blood-pool activity (obtained using patient blood samples) and the gamma ( $\gamma$ ) ray contribution, originating from the whole body activity (obtained using an uncollimated NaI detector). Because the rates of radioiodine absorption and release for the blood and for the whole body can be different, the corresponding cumulative activities differ as well. Given the mean energy per disintegration ( $\bar{E}$ ) and the absorbed fraction ( $\phi$ ), the maximum permissible activity is given by the following equation:

$$A_{\max} = 2\text{Gy} / [(\bar{A}\Delta)_{\beta} + (\bar{A}\phi\Delta)_{\gamma}] / A_{\text{tracer}}, \quad \text{Eq. 1}$$

assuming a linear uptake of iodine and local deposition of electron energy. Previously, the total number of disintegrations ( $\bar{A}$ ) was obtained using the method published by Benua et al. (1) and Harbert (4), where cumulative blood and whole body activities were obtained using a piecewise fit of each data pair with a single exponential decay. The number of disintegrations from the moment of ingestion until the first blood activity measurement is calculated assuming radioiodine is distributed instantaneously in 5 L of blood. The number of disintegrations beyond the last blood sample measurement is obtained assuming only physical clearance. The absorbed dose contribution for gamma rays is obtained using  $\bar{g}$ , a height- and mass-dependent mean total body geometric factor for  $^{131}\text{I}$  (8).  $\bar{g}$  values are only available for  $^{131}\text{I}$  and were obtained using outdated energy absorption coefficients (8,9). In addition, for children (height <140 cm or weight <40 kg) and for large patients (height >200 cm or

Received Oct. 21, 1997; revision accepted May 6, 1998.

For correspondence or reprints contact: Eli E. Furhang, PhD, Department of Medical Physics, Memorial Sloan Kettering Cancer Center, 1275 York Ave., New York, NY 10021.

weight >100 kg) it is necessary to extrapolate outside the  $\bar{g}$  data range, where accuracy is unknown.

It is also desirable to determine the absorbed dose to each lesion so that tumor doses can be prescribed directly, as in external beam radiotherapy, for those cases in which tumor uptake is high (>1%). The activity taken up in a lesion can be determined using two approaches. The first and fastest method uses a neck probe. This is a collimated NaI scintillation detector that is placed at a reproducible distance from the neck. Counts are converted to lesion activity by comparing counts from the neck with those from a known standard within a neck phantom. Lesion activity can also be determined from gamma camera images of the neck in the presence of a known standard. In this method, regions of interest (ROIs) are drawn on anterior images around the lesion standard and background. Lesion activity is given by the ratio of background corrected counts of the lesion relative to the standard. The absorbed dose to a lesion of mass (m) is determined by the following equation:

$$D_{\text{lesion}} = \Delta_{\beta} \bar{A} / m. \quad \text{Eq. 2}$$

The photon-absorbed dose contribution to  $D_{\text{lesion}}$  is neglected because of the small size of most thyroid lesions. The existing methodology (4) assumes  $\bar{A}$  to be the area under a single exponential decay, fixed by a measurement of thyroid activity at 24 h and a subsequent one at either 48 or 72 h, to determine the effective half-life ( $T_{1/2}$ ) for radioiodine clearance:

$$\bar{A} = A_{24} T_{1/2} / \ln(2). \quad \text{Eq. 3}$$

The objective of this work was to develop a system that will determine both  $A_{\text{max}}$  and  $D_{\text{lesion}}$  using the entire available kinetic data set. This was achieved by least-square, activity-weighted, fitting of uptake and clearance parameters to the time-activity data of each patient. Furthermore, we extended the dosimetry approach to include the use of other radioiodines either as tracers or therapy agents. This was accomplished by generating a photon-absorbed fraction table for  $^{123}\text{I}$ ,  $^{124}\text{I}$ ,  $^{125}\text{I}$  and  $^{131}\text{I}$  by a Monte Carlo simulation. The algorithm was developed as a spreadsheet (Microsoft Excel, Waltham, MA) for ease of use and will be made available to interested centers.

## MATERIALS AND METHODS

### Patient Preparation

Standard preparation of patients before  $^{131}\text{I}$  studies or therapy was described previously (10). Briefly, patients were hypothyroid with thyroid-stimulating factor levels >25  $\mu\text{U/mL}$  and were on a low-iodine diet. Patients were then orally administered a tracer activity of  $^{131}\text{I}$  (37–185 MBq).

### Dose-Limiting Activity ( $A_{\text{max}}$ )

**Absorbed Dose from  $\beta$  Particles.** One milliliter of heparinized blood samples was collected at 4, 24, 48, 72 and 96 h after ingestion. After the last blood sample was obtained, samples and a standard source were counted in a well-counter (LKB; Wallac,

Turku, Finland).  $^{133}\text{Ba}$  (peak energy = 356 keV), rather than  $^{131}\text{I}$  (peak energy = 364 keV), was used as the standard to decrease the uncertainties associated with dispensing 18.5 KBq in a busy radiopharmacy having background levels similar to the amount dispensed. Furthermore, the long half-life (10.74 y) of  $^{133}\text{Ba}$  eliminates fluctuations caused by the weekly  $^{131}\text{I}$  random dispensing variations.  $^{133}\text{Ba}$  also serves to confirm the  $^{131}\text{I}$  window settings, because the broader peak of  $^{133}\text{Ba}$  is more sensitive to variations in the energy calibration of the well counter. The counting efficiency difference within the energy window setting of 293–473 keV was quantified by comparing the  $^{133}\text{Ba}$  standard with a set of commercial  $^{131}\text{I}$  standards (Syncor, Mobile, AL) and establishing the conversion ratio as follows:

$$^{131}\text{C}_{^{133}\text{Ba}} = (\text{CPM/MBq})_{^{131}\text{I}} / (\text{CPM/MBq})_{^{133}\text{Ba}}, \quad \text{Eq. 4}$$

where CPM/MBq is the detector response normalized to source activity, and the subscript denotes the source. Given the sample counts ( $\text{CPM}_{\text{blood}}$ ), the standard counts ( $\text{CPM}_{^{133}\text{Ba}}$ ) and the current  $^{133}\text{Ba}$  activity, the blood activity is obtained using the following equation:

$$A_{\beta} = \text{CPM}_{\text{blood}} (A_{^{133}\text{Ba}} / \text{CPM}_{^{133}\text{Ba}})^{^{131}\text{C}_{^{133}\text{Ba}}}. \quad \text{Eq. 5}$$

Blood activity was fitted to a dual exponential clearance as follows:

$$A(t) = A_1 e^{-\lambda_1 t} + A_2 e^{-\lambda_2 t}. \quad \text{Eq. 6}$$

Fitting, or choosing the appropriate parameters, was performed by creating a spreadsheet (Microsoft Excel) to vary  $A_1$ ,  $\lambda_1$ ,  $A_2$  and  $\lambda_2$  in the direction of the steepest gradient to minimize the following:

$$\sum_m [A(t_m) - A_{\text{measured}}(t_m)]^2 (A_{\text{measured}}(t_m))^{1/2}, \quad \text{Eq. 7}$$

where  $t_m$  was the measurement time. The cumulative activity ( $\bar{A}$ ) was obtained by analytically integrating the area under the following activity fit:

$$\bar{A} = \int_0^T A dt = A_1 (1 - e^{-\lambda_1 T}) / \lambda_1 + A_2 (1 - e^{-\lambda_2 T}) / \lambda_2, \quad \text{Eq. 8}$$

where  $T$ , the time at which  $A = 0$ , is as follows:

$$T = [\ln(-A_2/A_1)] / (\lambda_2 - \lambda_1). \quad \text{Eq. 9}$$

Because 1 mL (~1 g) of blood was drawn, the  $\beta$ -absorbed dose-per-tracer activity is as follows:

$$(D/A_{\text{tracer}})_{\beta} = \bar{A}_{\beta} \Delta_{\beta} / A_{\text{tracer}}(t_{\text{reading}}), \quad \text{Eq. 10}$$

where  $\Delta_{\beta}$  is the electron equilibrium dose constants of the therapeutic radioiodine and where  $A_{\text{tracer}}(t_{\text{reading}})$  is the tracer activity at the time of the sample reading.

**Absorbed Dose from Gamma Rays.** Patients were seated on a stool 3.5 m away from an uncollimated NaI detector while anterior and posterior counts (1 min each) were obtained at 5 min and 2, 4, 24, 48, 72 and 96 h. A  $^{131}\text{I}$  standard was placed in the same geometry after each patient reading for system calibration and constancy check. The whole body clearance was obtained from the decrease in patient counts, adjusted by the standard counts that

correct for physical decay and daily fluctuations in detector response. The total body cumulative activity was obtained as described above (see equations 6–9). The photon-absorbed dose-per-unit tracer activity was obtained from the following equation:

$$(D/A_{\text{tracer}})_{\gamma} = \bar{A}_{\gamma} \Delta_{\gamma} \phi / (A_{\text{tracer}} M), \quad \text{Eq. 11}$$

where M is the body mass (in grams).

The photon-absorbed fractions were calculated for  $^{123}\text{I}$ ,  $^{124}\text{I}$ ,  $^{125}\text{I}$  and  $^{131}\text{I}$  by Monte Carlo simulation. The patient geometry was represented as a unit density water ellipsoid having the patient height, width and thickness. For each radionuclide, initial photons were generated uniformly inside the ellipsoid with a random direction and with energies sampled from a published decay scheme (7). Particle transport (for both photons and secondary electrons) was performed using the EGS4 transport code (11). Particle histories were terminated on crossing the ellipsoid surface or when the particle energy fell below 10 keV (i.e., thresholds were set at ECUT = 0.521 MeV and PCUT = 0.01 MeV for electrons and photons, respectively.) The energy deposited within the ellipsoid was obtained by scoring the energy deposited along secondary electron tracks. The ratio of the energy deposited within the ellipsoid to the energy emitted yields the absorbed fraction. Simulations were performed beyond 50,000 histories until the absorbed fraction SD was <1%. To avoid having to perform a Monte Carlo simulation for each patient, absorbed fractions were calculated once for 50–240-cm-high ellipsoids varying in width between one sixth to two fifths of the height and in thickness between one ninth to two fifths of the height (thickness was further limited to be less than or equal to the width). Ellipsoid height, width and thickness varied in 2-cm increments. For example, four 100-cm-high ellipsoids were generated having a width of 18 cm and thickness of 12, 14, 16 and 18 cm. Similarly, five 100-cm-high ellipsoids were generated having a width of 20 cm and thicknesses of 12, 14, 16, 18 and 20 cm. Calculations were repeated for each radioiodine, and the absorbed fractions were stored as separate data files. Given the desired radionuclide and the patient dimension, the appropriate data file was opened, and a linear interpolation was performed using the nearest eight ellipsoids. Absorbed fractions calculated in this work were compared with absorbed fractions as calculated with the Medical International Radiation Dose (MIRD) pamphlet no. 3 (12) in Table 1, for similar geometry and simulation

**TABLE 1**  
Ratios of Absorbed Fractions Calculated in this Study  
and in MIRD Pamphlet no. 3\*

Weight (kg)	Absorbed fraction <i>this study</i> / Absorbed fraction <i>MIRD 3</i>			
	0.02 MeV		0.364 MeV	
	Tissue	Water	Tissue	Water
2	1.07	1.08	1.13	1.15
4	1.04	1.06	1.05	1.03
6	1.03	1.04	1.03	1.02
60	1.01	1.02	1.00	1.01
70	1.01	1.02	1.01	1.03
100	1.01	1.02	1.02	1.02
160	1.01	1.01	1.00	1.02
200	1.00	1.01	1.00	0.99

\*The principal axes of the ellipsoids are in the ratio of 1:1.8:9.27.

conditions [1 SD, 10 keV threshold, same ellipsoid size and MIRD 5 composition (13)]. The MIRD 3 values are within 1 SD of the calculations presented in this report, except for small ellipsoids, where the absorbed fraction should be strongly dependent on the attenuation coefficients. These differences probably stem from the use of different sets of absorption coefficients (11,14). The higher carbon, lower oxygen tissue composition (23% carbon and 63% oxygen in this study (13) versus 15% carbon and 71% oxygen in MIRD 3) and hence the lower effective atomic number do not account for the discrepancy, because lower atomic number generally implies a lower absorbed fraction, especially at low energies. However, absorbed fractions calculated in this study are higher than the MIRD 3 values, and this discrepancy is greater at 364 keV than at 20 keV. Finally, Table 1 compares absorbed fractions obtained using water as a medium with the MIRD 3–absorbed fractions. No significant differences in the absorbed fractions were obtained between tissue and water as the transport medium. Therefore, water was used as the transport medium for absorbed fraction calculations.

**Lesion Dose ( $D_{\text{lesion}}$ ).** Lesion activity was obtained from a thyroid probe. To minimize contributions from the submandibular salivary glands, further collimation was added to the thyroid probe, reducing the original 20 cm FWHM to 10 cm. Neck counts are converted to lesion activity by comparing the neck counts with the counts of a known standard within a neck phantom. Lesion activity was also obtained from anterior neck scans using a gamma camera (Genesys; ADAC Laboratories, Inc., Milpitas, CA). ROI were drawn over the lesion for each time point. The counts obtained were converted to activity ( $A_{\text{measured}}$ ) by scaling with a  $^{131}\text{I}$  Petri dish standard of known activity placed in the camera field of view.

Activity measurements were obtained at 2, 4, 24, 48 and 72 h after tracer administration, using both a neck probe and gamma camera. The additional 2- and 4-h images were needed to quantitate the patient uptake phase, which occurs within the first 24 h. They also proved useful in determining the salivary gland uptake and assessing potential complications from high-dose radioiodine therapy (15). The cumulative lesion activity was obtained by fitting the iodine uptake and clearance with the following equation:

$$A(t) = A_0(1 - e^{-\lambda_{\text{rise}}t})e^{-\lambda_{\text{decay}}t} \quad \text{Eq. 12}$$

and solving for  $A_0$ ,  $\lambda_{\text{rise}}$  and  $\lambda_{\text{decay}}$  in the same manner as described in equation 7. The cumulative activity was obtained by analytically integrating the area under the fitted activity as follows:

$$\bar{A} = \int_0^{\infty} A(t)dt = \frac{A_0 \lambda_{\text{rise}}}{\lambda_{\text{decay}}(\lambda_{\text{decay}} + \lambda_{\text{rise}})} \quad \text{Eq. 13}$$

Assuming a linear iodine uptake and a negligible  $\gamma$ -absorbed dose contribution, the lesion absorbed dose is given by the following equation:

$$D_{\text{lesion}} = \frac{\Delta_{\beta}}{m_{\text{lesion}}} \times \left( \bar{A} \times \frac{A_{\text{max}}}{A_{\text{tracer}}} \right), \quad \text{Eq. 14}$$

where  $m_{\text{lesion}}$  is the lesion mass. For large (>10 g) tumors, mass estimates can be obtained from the gamma camera, CT or ultrasonography images. Lesion sizes between 1 and 10 g may be obtained with greater accuracy from  $^{124}\text{I}$  PET imaging (16). At <1 g, the dosimetric uncertainties associated with lesion mass are unknown. Nevertheless, in these cases, the principle objective is to

deliver the maximum possible dose consistent with bone marrow tolerance. In this study, the dose to small lesions was calculated using an assumed 1 g mass, which would conservatively underestimate the tumor dose.

## RESULTS

### Maximum Permissible Activity ( $A_{max}$ )

Three modifications were implemented to the conventional technique to determine  $A_{max}$ . The impact of each is described below.

**Initial Blood Activity.** The cumulative blood activity was calculated using the empirical assumption that the initial blood activity is distributed instantaneously in 5 L and compared with the new method that involves a fit to blood samples from 2–96 h, as described above. Ratios of  $A_{max}$  calculated without and with the initial blood activity assumption are shown in Fig. 1A. The two methods produced similar results (<10% differences) for 11 of 14 patients, when the initial activity predicted by the fit matched the assumed value and when the last measured value was small.

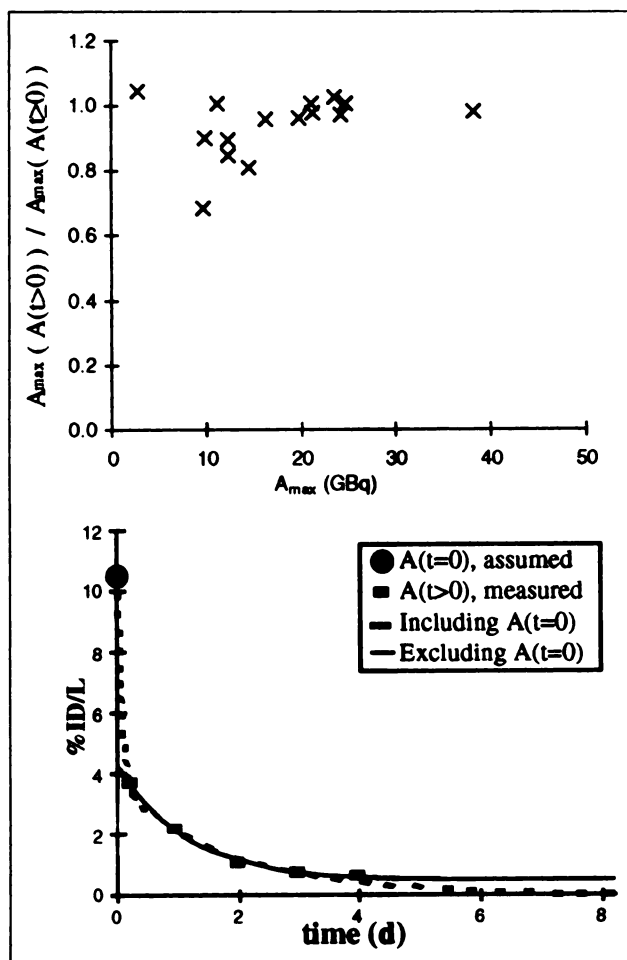


**FIGURE 1.** (A) Ratios of  $A_{max}$  calculated with and without assumed  $A(t=0)$  for 14 patients. (B) Blood activity fit including and excluding  $A(t=0)$  obtained by assuming activity to be immediately distributed in 5 L of blood.

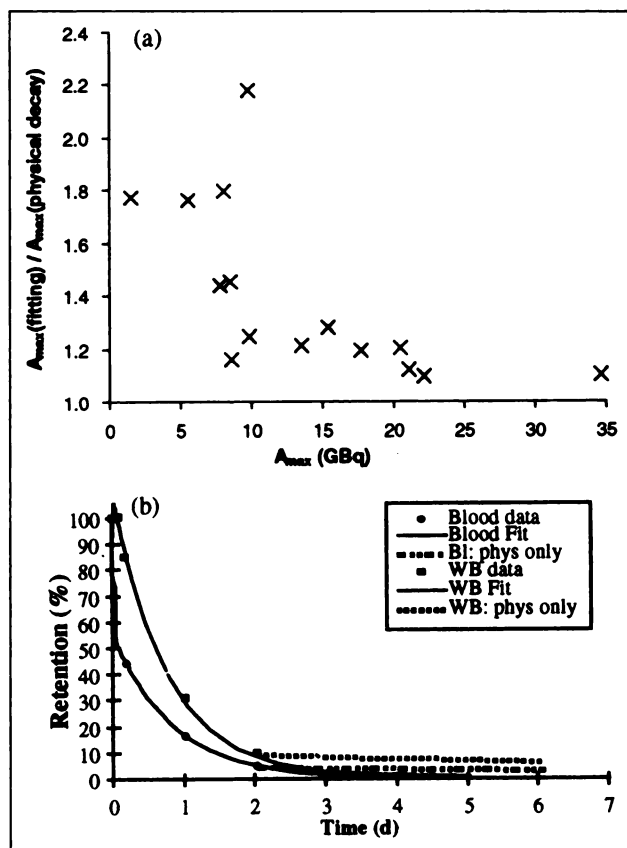


**FIGURE 2.** (A) Ratios of  $A_{max}$  calculated using fitting and assuming physical decay beyond last data point for 14 patients. (B) Blood and whole body fits using measured values. Also shown is physical decay beyond last data point, which is assumed in classical approach.

However, in slow clearance cases with a discrepancy between assumed and predicted initial activity (as shown in Fig. 1B), the small area increment resulting from the incorporation of a large initial value is outweighed by the consequential large decrease in the tail portion of the curve, because the large weight of the initial activity (weight  $\sim 1/\sigma = A^{1/2}$ ) forces the fit to clear faster. Ignoring the initial activity assumption in such cases was found to increase  $\bar{A}_\beta$ .

**TABLE 2**  
Ratios of Gamma Ray Dose Calculated Using Absorbed Fractions and Using  $\bar{g}$

Height (cm)	Width (cm)	Thickness (cm)	$D_\gamma(\text{using } \phi) / D_\gamma(\text{using } \bar{g})$
61	15	12	0.81
91	18	13	0.89
173	34	25	1.06
173	40	37	1.05
191	38	25	1.05
210	45	32	1.02

$\gamma$  = gamma ray;  $\phi$  = absorbed fraction;  $\bar{g}$  = height and mass-dependent mean total body factor for  $^{131}\text{I}$ .

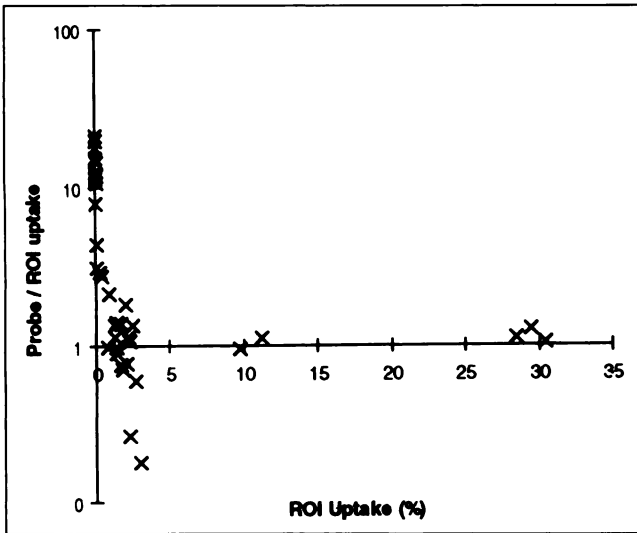


**FIGURE 3.** Ratio of probe to ROI 24-h percent uptake for 38 patients as function of percent ROI uptake.

by as much as 30%, entailing a lower permissible  $A_{max}$ , which will deliver a lower blood dose.

**Physical Decay Beyond the Last Data Point.** Cumulative blood and whole body activities were calculated with and without assuming physical decay beyond the last data point, and the results are shown in Fig. 2A. The two methods produced similar results when the last data point approached zero or when the last few data points decayed with the physical half-life (as in the case of kidney dysfunction). However, when the last data point does not approach zero (Fig. 2B), incorporating the biological decay yielded up to 50% smaller cumulative activities, resulting in a 50%

greater permissible  $A_{max}$  and a correspondingly larger blood dose.

**Use of the Geometrical Factor  $\bar{g}$ .** Photon-absorbed dose-per-tracer activity calculated using  $\bar{g}$  and absorbed fractions are compared in Table 2 for representative body sizes. Values outside the available  $\bar{g}$  range were obtained using the following equation:

$$\bar{g} = 77.52 + 42.42 \times \text{weight}^{0.8356} \times \text{height}^{-0.6590}, \quad \text{Eq. 15}$$

where the parameters were obtained by fitting the available  $\bar{g}$  values. As can be observed in Table 2, the largest absorbed dose discrepancies were observed for children. However, it seems that the fit described by equation 15 is sufficiently accurate for patients having dimensions greater than the available  $\bar{g}$  range.

### Lesion Dose ( $D_{lesion}$ )

The activity of radioiodine within lesions in the neck was measured on each successive day using both a thyroid probe and a gamma camera. Probe to ROI uptake ratios are plotted in Fig. 3. When the lesion uptake in the neck is large ( $>5\%$ ), both methods produce similar uptake values. However, for lesions having  $<1\%$  uptake, the probe can yield uptake values much different than those obtained using the ROI method. Most commonly, the probe yields higher uptake values (up to 20 times greater). This stems from radioiodine in the blood pool rather than the lesion. In some cases, the probe yielded lower uptake values (as much as 5 times smaller), which we attributed to the increased probability of detector mispositioning associated with the additional collimation used in this study. However, the penalty of using the original large-field-of-view collimator is overestimating

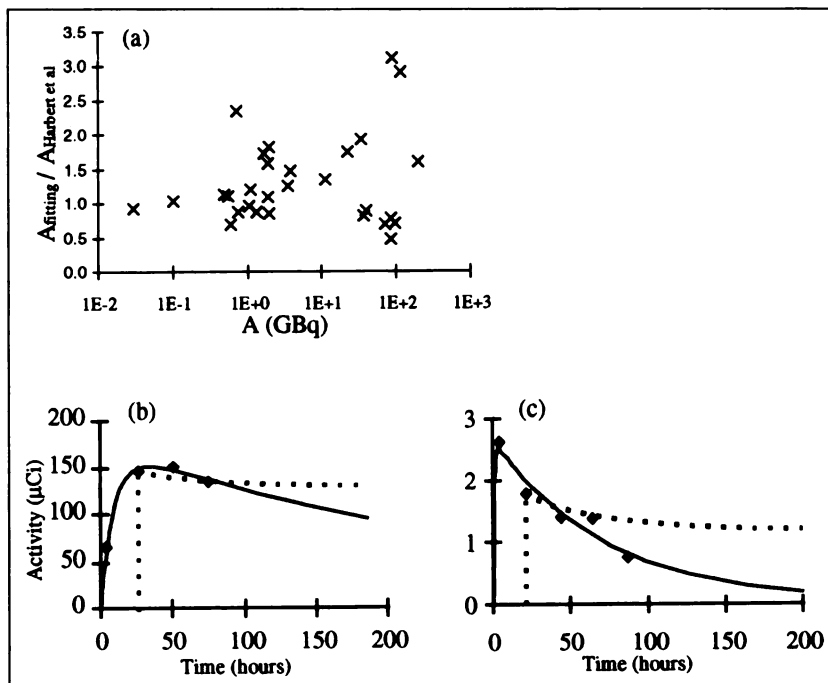


**FIGURE 4.** (a) Ratio of lesion activity calculated using fitting and using method of Harbert (4). Lesion activity ( $\blacklozenge$ ) as function of time. Cumulative lesion activity is obtained using both fits (—) and using assumption that patient activity peaks at 24 h (- - -). (b) shows patient whose uptake follows the assumption, whereas (c) shows activity of patient whose uptake peaks within 2 h.

uptake values because of counts from the submandibular and salivary glands. Furthermore, lesion-absorbed doses calculated using the thyroid probe can be doubly erroneous, because the probe clearance data reflects averaged clearances from all the iodine that is in tissues within the field of view.

Lesion activities, calculated using the ROI method, were used to estimate  $D_{\text{lesion}}$ . Calculations were repeated using both fitting and classical formalism, where the decay rate is obtained from the 24- and 72-h activities and the 24-h activity is substituted for the initial activity (4). As is shown in Fig. 4A, the classic approach yielded a similar answer in cases where the activity peaks at about 24 h, probably because the missing area under the uptake curve is partially compensated by the slower clearance inferred from the 24–72-h decay curve (Fig. 4B). However, when the patient activity peaks at a different time (for example, 2 h in Fig. 4C), cumulative activities calculated using the classic formalism would overestimate both  $\bar{A}$  and  $D_{\text{lesion}}$  by a factor of 3.

## DISCUSSION

The thyroid cancer dosimetry method presented in this report incorporates the individual patient uptake and clearance of radioiodine. It permits dosimetry to be performed with alternative radioiodines ( $^{123}\text{I}$ ,  $^{124}\text{I}$  and  $^{125}\text{I}$ ) as tracers or as therapeutic agents. The implications of estimating the maximum permissible activity using the method of Benua et al. (1) relative to the fitting procedure described in this report were evaluated. For approximately 80% of the patients, the maximum tolerated activity calculated by the traditional method of Benua et al. (1) and the fitting method presented here were within 10% agreement. However, for 20% of the patients, the differences were greater. The assumption that the initial blood activity is distributed instantaneously in 5 L was found to introduce an error in  $A_{\text{max}}$  of up to 30%, whereas assuming physical decay beyond the last data point introduced an error of up to 50%.

Thyroid lesion uptake was evaluated using both a thyroid probe and gamma camera images. It was found that the use of a neck probe could overestimate lesion uptake by more than an order of magnitude when the percent injected uptake is <1%. We therefore recommend that an ROI analysis be used to determine lesion uptakes for patients with thyroid

cancer who commonly have low uptake. The conventional thyroid lesion dose calculation using two uptake points (4) could overestimate  $D_{\text{lesion}}$  by up to a factor of 3 when compared with the method of fitting five data points at 2, 4, 24, 48 and 72 h beyond uncertainties associated with the lesion mass. Acquiring five measurements is often logistically strenuous and, when it is necessary to reduce the number of points, at least one measurement must be obtained at the uptake phase (2–4 h), an additional measurement during the typical peak time (24 h) and a final measurement as late as possible (72–96 h).

## REFERENCES

1. Benua RS, Cicale NR, Sonenberg M, Rawson RW. The relation of radioiodine dosimetry to results and complications in the treatment of metastatic thyroid cancer. *AJR*. 1962;87:171–182.
2. Maxon HR, Englaro EE, Thomas SR, et al. Radioiodine-131 therapy for well-differentiated thyroid cancer—a quantitative radiation dosimetric approach: outcome and validation in 85 patients. *J Nucl Med*. 1992;33:1132–1136.
3. Maxon HR. The role of  $^{131}\text{I}$  in the treatment of thyroid cancer. *Thyroid Today*. 1993;2:1–8.
4. Harbert JC. *Nuclear Medicine Therapy*. New York, NY: Thieme Medical; 1987.
5. Samuel AM, Rajashekhara B. Radioiodine therapy for well-differentiated thyroid cancer: a quantitative dosimetric evaluation for remnant thyroid ablation after surgery. *J Nucl Med*. 1994;35:1944–1950.
6. Zanzonico PB, Brill AB, Becker DV. Radiation dosimetry. In: Wagner HN, Szabo Z, Buchanan JW, eds. *Principles of Nuclear Medicine*. 2nd edition. Philadelphia, PA: Saunders; 1995:106–134.
7. Weber DA, Eckerman KF, Dillman LT, Ryman JC. *MIRD: Radionuclide Data and Decay Schemes*. New York, NY: Society of Nuclear Medicine; 1989.
8. Hine JG, Brownell GL. *Radiation Dosimetry*. New York, NY: Academic Press; 1956:858.
9. Bush F. The integral dose received from a uniformly distributed radioactive isotope. *Br J Radiol*. 1949;22:96–102.
10. Mazzaferri EL, Jhiang SM. Long-term impact of initial surgical and medical therapy on papillary and follicular thyroid cancer. *Am J Med*. 1994;97:418–428.
11. Nelson WR, Hirayama H, Rogers DWO. *The EGS4 Code System. SLAC Report 265*. Springfield, VA: National Technical Information Service; 1985.
12. Brownell GL, Ellett WH, Reddy AR. MIRD pamphlet 3: absorbed fractions for photon dosimetry. *J Nucl Med*. 1968;9:27–39.
13. Snyder WS, Ford MR, Warner GG. *MIRD Pamphlet 5 (revised): Estimates of Specific Absorbed Fractions for Photon Sources Uniformly Distributed in Various Organs of a Heterogeneous Phantom*. New York, NY: Society of Nuclear Medicine; 1978.
14. Storm E, Israel HI. Photon cross sections from 1 keV to 100 MeV for elements  $Z=1$  to  $Z=100$ . *Atomic Data and Nuclear Data Tables*. 1970;7:565.
15. Imbriaco M, Furhang EE, Humm JL, et al. Radiation dose to the salivary glands during I-131 treatment of thyroid cancer: correlation with clinical findings [abstract]. *J Nucl Med*. 1997;38:230P.
16. Erdi YE, Macapinlac H, Larson SM, Yeung H, Furhang EE, Humm JL. Thyroid therapy treatment planning using positron emission tomography (PET). *Med Phys*. 1997;24:970.